Human Molecular Genetics, 2014, Vol. 23, No. 25 **6878–6893**
doi:10.1093/hmg/ddu410
Advance Access published on August 7, 2014

Deactivation of TBP contributes to SCA17 pathogenesis

Tun-Chieh Hsu[1], Cheng-Kuang Wang[2], Chun-Yen Yang[1], Li-Ching Lee[1], Hsiu-Mei Hsieh-Li[1], Long-Sun Ro[3], Chiung-Mei Chen[3], Guey-Jen Lee-Chen[1] and Ming-Tsan Su[1,*]

[1]Department of Life Science, National Taiwan Normal University, Taipei 11677, Taiwan, [2]Department of Laboratory Medicine, Jen-Teh Junior College of Medicine, Nursing and Management, Miaoli 35664, Taiwan and [3]Department of Neurology, Chang Gung Memorial Hospital, College of Medicine, Chang-Gung University, Taoyuan 33305, Taiwan

Received June 6, 2014; Revised July 27, 2014; Accepted August 4, 2014

Spinocerebellar ataxia type 17 (SCA17) is an autosomal dominant cerebellar ataxia caused by the expansion of polyglutamine (polyQ) within the TATA box-binding protein (TBP). Previous studies have shown that polyQ-expanded TBP forms neurotoxic aggregates and alters downstream genes. However, how expanded polyQ tracts affect the function of TBP and the link between dysfunctional TBP and SCA17 is not clearly understood. In this study, we generated novel *Drosophila* models for SCA17 that recapitulate pathological features such as aggregate formation, mobility defects and premature death. In addition to forming neurotoxic aggregates, we determined that polyQ-expanded TBP reduces its own intrinsic DNA-binding and transcription abilities. Dysfunctional TBP also disrupts normal TBP function. Furthermore, heterozygous *dTbp* amorph mutant flies exhibited SCA17-like phenotypes and flies expressing polyQ-expanded TBP exhibited enhanced retinal degeneration, suggesting that loss of TBP function may contribute to SCA17 pathogenesis. We further determined that the downregulation of TBP activity enhances retinal degeneration in SCA3 and Huntington's disease fly models, indicating that the deactivation of TBP is likely to play a common role in polyQ-induced neurodegeneration.

INTRODUCTION

Thus far, 10 neurodegenerative diseases, including the spinocerebellar ataxias (SCAs) SCA1, SCA2, SCA3, SCA6, SCA7, SCA8 and SCA17, Huntington's disease (HD), dentatorubral and pallidoluysian atrophy (DRPLA) and spinobulbar muscular atrophy, have been attributed to CAG-repeat sequence expansion in various unrelated genes, resulting in abnormally long polyglutamine (polyQ) tracts in encoded proteins. Although disease progression in these neuronal disorders is heterogeneous, common symptoms have been observed among these neurodegenerative diseases, indicating that similar pathomechanisms may exist. Because insoluble aggregates are prominent and common among such diseases, expanded polyQ-containing inclusion bodies are considered the primary cause of these diseases. Furthermore, studies have shown that expanded polyQ aggregates confer gain-of-toxicity functions by interacting aberrantly with organelles, including nuclei, endoplasmic reticula and mitochondria. In addition, expanded polyQ-containing proteins recruit and impair many cellular proteins, including molecular chaperones, components of the ubiquitin–proteasome system and transcription factors. Abnormal interactions among cell components that disrupt their associated functions are considered to contribute to the pathogenesis of polyQ-mediated neurodegeneration (1,2).

Because the polyQ tract is responsible for the oligomerization of polyQ-containing proteins and the formation of insoluble aggregates (3), several glutamine-rich proteins, including the cAMP response element-binding protein (CREB)-binding protein (CBP), specificity protein 1 (SP1) and TATA box-binding protein (TBP), are sequestered in expanded polyQ-containing aggregates (4–6). In addition, CBP and SP1 depletion were found to contribute to the pathogenesis of polyQ-mediated neurodegeneration (7,8). Among the glutamine-rich transcription factors implicated in polyQ-mediated neurodegeneration, TBP is notable (9). First, TBP is a general transcription factor that is essential in forming the transcription preinitiation complex and transcription of RNA polymerases I, II and III (Pol I, II and III). Aberrant TBP activity is expected to profoundly affect normal cellular function. The inactivation of TBP causes the downregulation of Pol I and Pol III

*To whom correspondence should be addressed at: Department of Life Science, National Taiwan Normal University, 88, Sec. 4, Ting-Chou Rd, Taipei 11677, Taiwan. Tel: +886 229336875; Fax: +886 229312904; Email: mtsu@ntnu.edu.tw

transcription, growth arrest and cell death in mice (10). Secondly, TBP is sequestered in several pathogenic polyQ inclusions, including expanded polyQ-Huntingtin (Htt), atrophin-1, ataxin-1 (Atx1) and ataxin-3 (Atx3), which cause HD, DRPLA, SCA1 and SCA3, respectively (5,11–13). Loss of TBP function has been posited to play a crucial role in the pathogenesis of these neuronal impairments. Nevertheless, the aforementioned hypothesis has not been tested. Finally, the expansion of polyQ tracts within the N-terminal domains (NTDs) of TBP was determined to cause autosomal dominant SCA17 (14–16). The glutamine-rich domain of TBP exhibits transactivation capability (17). PolyQ expansion has been shown to enhance TBP-dependent transcription and reduce TBP–DNA binding (18,19). Aberrant TATA-dependent transcriptional activity induced by polyQ-expanded TBP has been suggested to be neurotoxic; nevertheless, this viewpoint has not been thoroughly investigated.

Several disease models, including cell, *Drosophila* and mouse models, have been generated to elucidate the pathomechanisms of SCA17 (19–24). The overexpression of full-length-mutant TBP and truncated-mutant TBP that lacked DNA-binding domains (DBDs) was found to cause the formation of inclusions (18,19), suggesting that insoluble aggregates are causative factors and that the neurotoxicity of mutant TBP is DNA-binding-independent. Thus, the pathogenesis of SCA17 seems similar to that of other polyQ-mediated neuropathies. Studies have shown that expanded polyQ tracts affect TBP dimerization and TBP–TATA box complex formation (19,24): by enhancing the association of mutant TBP with general transcription factor IIB, the occupancy of both proteins on the Hspb1 promoter (24) is reduced. Consequently, downregulation of Hspb1 is considered to be linked to SCA17 pathogenesis (24). Mutant TBP also exhibits a strong affinity for transcription factors, including nuclear factor-Y and SP1 (20,25), and reduces the association of respective transcription factors with promoters of downstream genes such as TrkA, Hsp70, Hsp25, HspA5 and HspA8 (25). In addition, RBP-J/Su(H), a Q/N-rich transcription factor in Notch signaling, is selectively downregulated in *Drosophila* models of SCA17, because its interaction with polyQ-expanded TBP is stronger than that of wild-type TBP (21). Reductions in cellular Su(H) activity and Notch signaling modulate SCA17 progression (21). Recently, a study showed that mutant TBP decreased its association with XBP1s, reducing the expression of Purkinje cell-enriched mesencephalic astrocyte-derived neurotrophic factor (MANF) in SCA17-inducible knock-in mice (26). The overexpression of Hsc70 can restore the interaction between TBP and XBP1, and increasing MANF expression ameliorated mutant TBP-induced toxicity in SCA17 mice (26).

Although the aforementioned studies have addressed several SCA17 pathomechanisms, whether expanded polyQ tracts affect the function of TBP has yet to be comprehensively addressed. In addition, the link between malfunctioning TBP and SCA17 has not been addressed. In the present study, we generated novel *Drosophila* models for SCA17 by overexpressing polyQ-expanded TBP. In addition to forming neurotoxic aggregates as described in previous studies (19,24), we observed that polyQ-expanded TBP is dysfunctional. Moreover, the mutant TBP sequestered wild-type TBP in the neuroblasts of flies and impaired the normal function of wild-type TBP. We further revealed that loss of *Drosophila* TBP (*dTbp*) mutants exhibited SCA17-like phenotypes and polyQ-expanded TBP-induced degeneration was enhanced in *dTbp* mutant backgrounds. These results suggested that the deactivation of TBP may contribute to SCA17 pathogenesis. Most notably, we showed that reduced *dTbp* expression exacerbated retinal degeneration induced in polyQ-expanded SCA3 and HD fly models. The findings suggest that the dysfunction of TBP may play a universal role in polyQ-induced neurodegeneration.

RESULTS

Generating *Drosophila* models of SCA17

To generate a fly model of SCA17, expression constructs that comprised full-length human TBP with 36 (wild-type, TBP-36Q) and 109 (pathogenic allele, TBP-109Q) glutamine residues were introduced into the genome of *Drosophila* by using germ-line transformation. The target expression of transgenes was achieved using the UAS/gal4 binary expression system (27). Real-time polymerase chain reaction (PCR) and immunoblotting analyses revealed that the expression levels of TBP-36Q and TBP-109Q in the heads of the 1-day-old flies were comparable (Fig. 1A–C). Retinal overexpression of TBP-36Q driven by *Gmr*-gal4 (*Gmr*>TBP-36Q) did not cause age-dependent morphological defects in the eyes of the adult flies when compared with the control *Gmr*-gal4 driver group (Fig. 1D). The overexpression of TBP-109Q did not cause obvious morphological defects in the eyes of the adult flies at 3 weeks of age (Fig. 1D, w3). However, loss of pigment in the eyes of the 5-week-old adult flies expressing TBP-109Q was observed (Fig. 1D, w5). The depigmentation phenotype induced by TBP-109Q was more evident as age increased. A detailed examination of eye morphology by using scanning electronic microscopy (SEM) revealed that several eye phenotypes, including bristle loss and disorganization of ommatidial architecture, were present in TBP-109Q-expressing flies at 7 weeks of age (Fig. 1D). Compared with previous SCA17 fly models in which the overexpression of normal TBP (TBP-34Q) induces retinal degeneration in the eyes of newly eclosed flies (21), we believe that our SCA17 fly model is more representative because it exhibits a degenerative phenotype only in old age.

To investigate whether fly models exhibit mobility defects and high mortality rates, transgenes were expressed under the control of a pan-neuronal *Elav*-gal4 driver. We observed that the motor function of the control *Elav*-gal4 lines decreased with age in negative geotaxis assays (Fig. 1E). The motor function of the TBP-36Q-expressing flies (*Elav*>TBP-36Q) also declined with increasing age. The climbing index (CI) of *Elav*>TBP-36Q flies aged 40 days seemed lower than that of the control *Elav*-gal4 lines. However, statistical analysis indicated that this difference was nonsignificant ($P > 0.05$). In contrast to *Elav*>TBP-36Q flies, *Elav*>TBP-109Q flies did not initially exhibit mobility defects at 20 days of age. However, the mobility performance of the *Elav*>TBP-109Q flies was significantly lower than that of the control *Elav*-gal4 lines or *Elav*>TBP-36Q flies aged 40 days (Fig. 1E). In addition, the average lifespans of the control *Elav*-gal4, TBP-36Q- and TBP-109Q-expressing flies were 59, 51 and 46 days, respectively (Fig. 1F). Statistical analyses revealed that the neuronal overexpression of TBP-36Q reduced the lifespan of transgenic flies (log-rank test, $P < 0.05$). However, compared with the control *Elav*-gal4 and

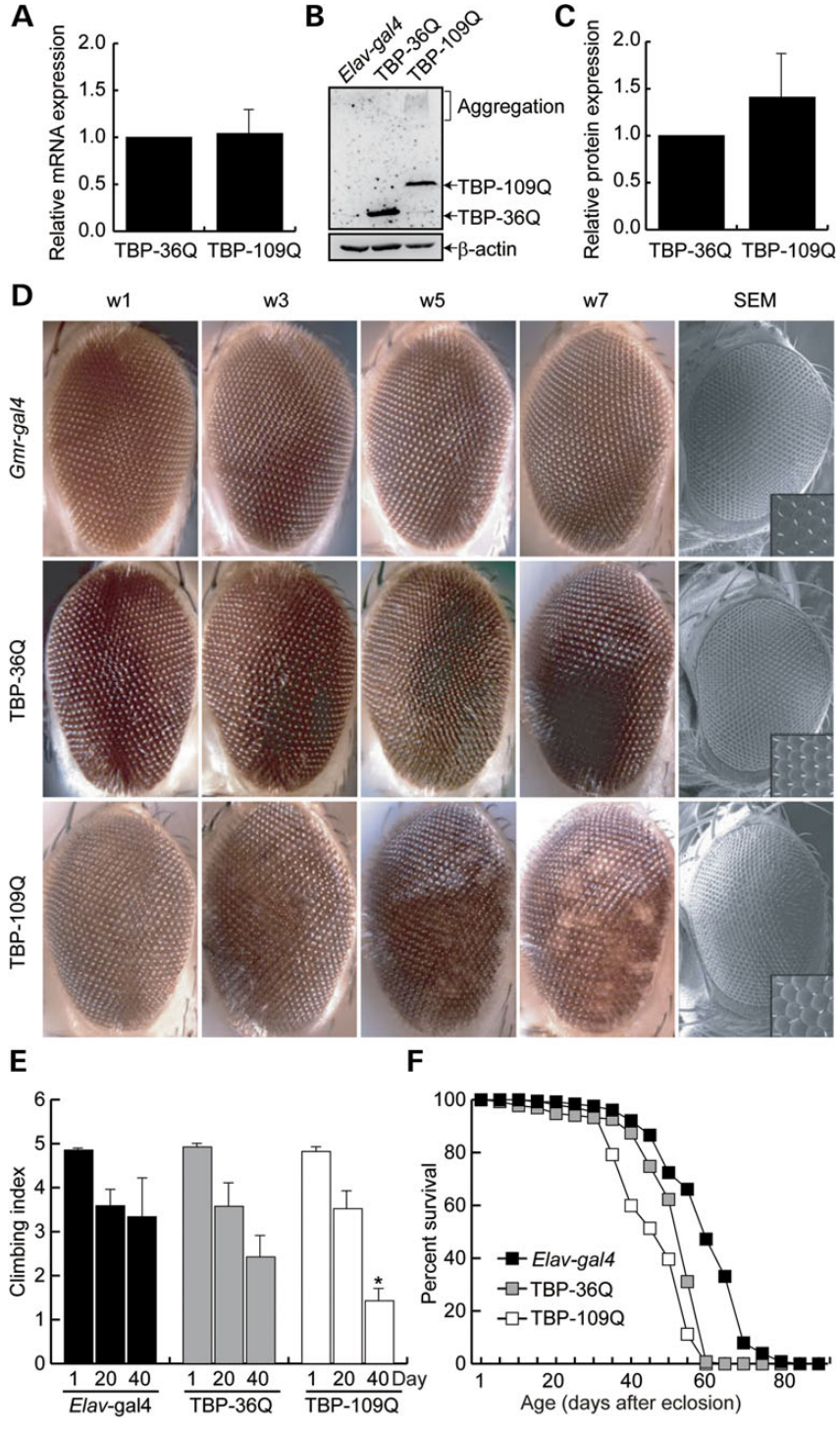

Figure 1. *Drosophila* model of SCA17. (**A**) Real-time PCR analysis of TBP mRNA expression in the heads of 1-day-old flies. (**B**) Representative immunoblot and relative protein expression levels of TBP-36Q and TBP-109Q in the heads of 1-day-old flies detected using 1TBP18 antibodies. Because the NTDs of TBP among vertebrates and invertebrates are highly diverse, and 1TBP18 recognizes an epitope within amino acid residues of mammalian TBPs, only human TBP was detected. (**C**) Relative protein expression was determined using chemiluminescence and normalized to the abundance of β-actin. The data were obtained from five independent experiments and are displayed as average arbitrary units ± SD. Soluble and aggregate TBP-109Q were counted as the total expression of TBP-109Q. No significant difference in the expression levels of TBP-36Q and TBP-109Q (Student's *t*-test, $P = 0.141$) was observed. (**D**) The eye morphologies of flies of various ages were determined from 1 to 7 weeks after eclosion (w1–w7). The eye morphologies of 7-week-old flies were analyzed in detail by using SEM (right panel). The insets exhibited an enlarged ommatidial architecture. The control *Gmr*-gal4 driver line (upper panel) and TBP-36Q-expressing flies (middle panel) did not exhibit the rough-eye phenotype throughout their entire lifespan. The TBP-109Q-expressing flies (lower panel) showed mild depigmentation in Week 5. (**F**) Negative geotaxis assays revealed mobility defects in the TBP-109Q-expressing flies at Day 40. Data are expressed as mean ± SD and statistical significance was determined using a Student's *t*-test ($^*P < 0.05, n = 100$). (F) The survival rate of the TBP-109Q-expressing flies was significantly reduced. Neuronal overexpressing TBP-36Q mildly reduced the longevity of flies compared with the control *Elav*-gal4 lines. The log-rank test was used for evaluating their lifespan ($n = 100$).

TBP-36Q-expressing flies, the lifespan of the TBP-109Q-expressing flies was significantly reduced ($P < 0.001$). Overall, the data suggested that the toxicity of TBP depends on polyQ length. Remarkably, the overexpression of TBP-36Q reduced the lifespan of transgenic flies (Fig. 1F). This result seems to agree with the finding that the retinal overexpression of human TBP-34Q causes mild eye degeneration in flies (21). Because TBP is a general transcription factor and is biologically active in *Drosophila* (21), ectopic TBP activity may dysregulate survival or apoptotic gene expression.

PolyQ-expanded TBP forms protein aggregation

The formation of intracellular inclusions is a pathological hallmark of polyQ-mediated diseases, including SCA17 (14,15,18,19,24). Filter trap assays were used to test whether polyQ-expanded TBP forms insoluble proteins *in vitro*. Because bacterially purified TBP-109Q is highly insoluble, TBP-36Q and TBP-109Q were fused with a N-terminal glutathione *S*-transferase (GST) tag, and a tobacco etch virus (TEV) protease cleaving site was inserted between the GST tag and TBP to increase solubility (Fig. 2A, GST-TBP). Soluble recombinant proteins were purified and digested using a TEV protease to initiate aggregation reactions. The reaction mixtures were filtered through 0.2-μm cellulose acetate membranes at various time points. The retained protein aggregates were probed using anti-TBP antibodies. As shown in Figure 2B, TBP-36Q did not form detectable protein aggregates *in vitro* after 17 h (Fig. 2B). In contrast, 3 h after initial TEV digestion, aggregates of TBP-109Q were detected (Fig. 2B). The formation of TBP-109Q aggregates increased as time increased and reached a maximum at ~17 h after treatment with the TEV protease (Fig. 2B).

To prove whether TBP-109Q forms protein aggregates *in vivo*, monoclonal 1C2 antibodies that recognize expanded polyQ epitopes were used to stain the eye discs of the *Elav*>TBP flies. Insoluble inclusions were not observed in the eye discs of the transgenic flies expressing TBP-36Q (Fig. 2C). However, TBP-109Q-containing protein aggregates were apparently detected in the eye discs of the flies (Fig. 2C). In addition, we compared the production of protein aggregates on Day 2 and in Weeks 1 and 3 in the heads of the *Elav*-gal4, *Elav*>TBP-36Q and *Elav*-109Q flies (Fig. 2D). Protein aggregates were not detected in the control *Elav*-gal4 or *Elav*>TBP-36Q between Day 2 and Week 3. In contrast, both soluble and insoluble TBP were detected in the 2-day-old flies expressing TBP-109Q (Fig. 2D). In the 1-week-old *Elav*>TBP-109Q flies, the soluble fraction disappeared and insoluble aggregates increased (Fig. 2D, see stacking gel). By Week 3, aggregates were clearly observed in the heads of the *Elav*>TBP-109Q flies (Fig. 2D). These results showed that the formation of aggregates is polyQ- and age-dependent (Fig. 2D). Overall, we showed that our fly models recapitulated several pathological hallmarks of SCA17, including age-dependent degeneration, mobility defects and a shortened lifespan.

PolyQ expansion affects the intrinsic function of TBP

In addition to forming protein aggregates that cause neurodegeneration, we suspected that polyQ expansion within TBP may

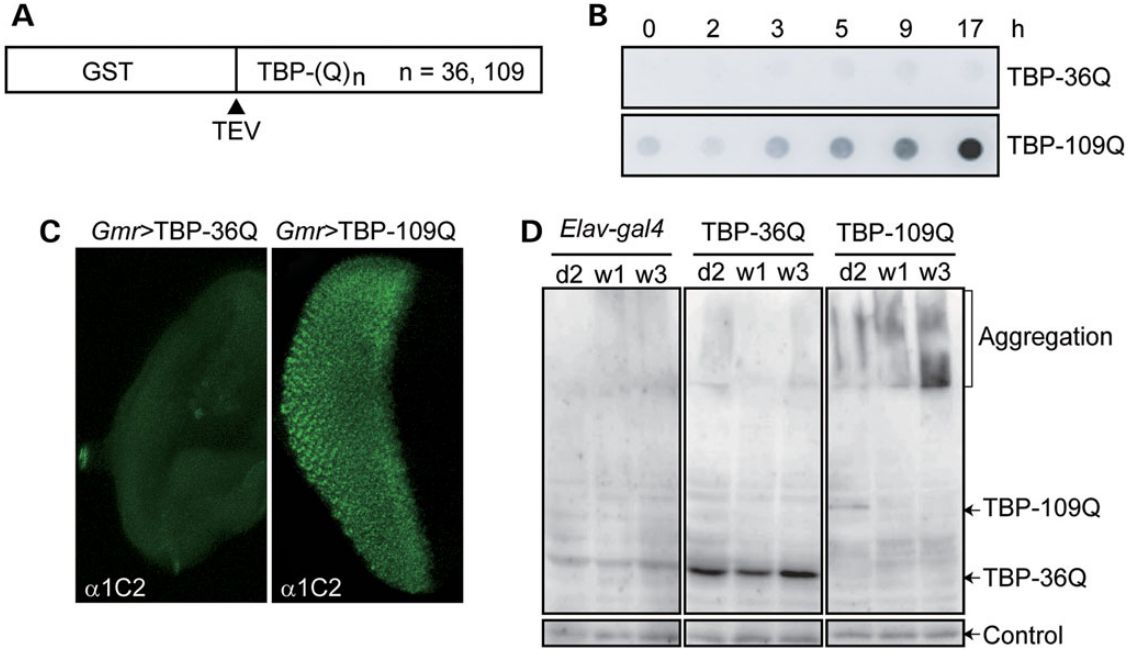

Figure 2. PolyQ-expanded TBP forms insoluble inclusions. (**A**) Schematic representation of the recombinant GST-TBP protein used in the filter trap assay. The black arrow head represents the cleavage site for the TEV protease. (**B**) 1C2 antibodies were used for detection, and TBP-36Q did not form SDS-insoluble protein aggregates (upper panel). TBP-109Q formed insoluble aggregates 3 h after TEV digestion *in vitro* (lower panel). The formation of aggregates was time-dependent and reached a plateau at 17 h. (**C**) 1C2 antibodies were used for detection, and insoluble inclusions were not detected in the eye discs of the TBP-36Q-expressing flies. Protein aggregates were observed in TBP-109Q-expressing flies' eye discs, driven by *Gmr*-gal4. (**D**) Western blot analysis showed that SDS-insoluble aggregation was not detected in the heads of the *Elav*-gal4 and TBP-36Q-expressing flies with anti-TBP antibodies. Protein aggregation was profoundly increased in the heads of the aged TBP-109Q-expressing flies. Minor levels of soluble TBP-109Q protein were detected in 2-day-old TBP-109Q flies. Soluble TBP-109Q was completely abolished, whereas aggregates were detected in stacking gel. Nonspecific protein bands showed equal loading in the samples (control).

alter TBP function, causing SCA17. To test this hypothesis, we conducted electrophoretic mobility shift assays (EMSAs) to examine whether the DNA-binding ability of TBP was affected by the expansion of the polyQ tract. Labeled TATA DNA probes were incubated with GST-TBP recombinant proteins (Fig. 2A), and binding reactions were initiated by cleaving with TEV proteases. The binding of TBP-36Q to TATA box DNA attained a maximum within 1 h (Fig. 3A). A prolonged reaction time did not increase the formation of TBP–DNA complexes (Fig. 3A). Remarkably, TBP-109Q nearly lost its DNA affinity completely within 1 h of the initiation of the binding reaction (Fig. 3A). The DNA affinity of TBP-109Q was time-dependent and diminished gradually (Fig. 3A). As mentioned, TBP-109Q formed obvious protein aggregates at ~3 h *in vitro* (Fig. 2B) and nearly completely lost its DNA affinity within 1 h (Fig. 3A), indicating that TBP-109Q in its soluble state is dysfunctional.

To quantify comprehensively how polyQ expansion affects the DNA-binding ability of TBP, liquid chemiluminescent DNA pull-down assays were conducted (28). Briefly, soluble TBPs bound to magnetic beads were incubated with biotinylated TATA DNA in binding reactions for 1 h. TBP-bound DNA was captured using a magnet. The amount of bound DNA was

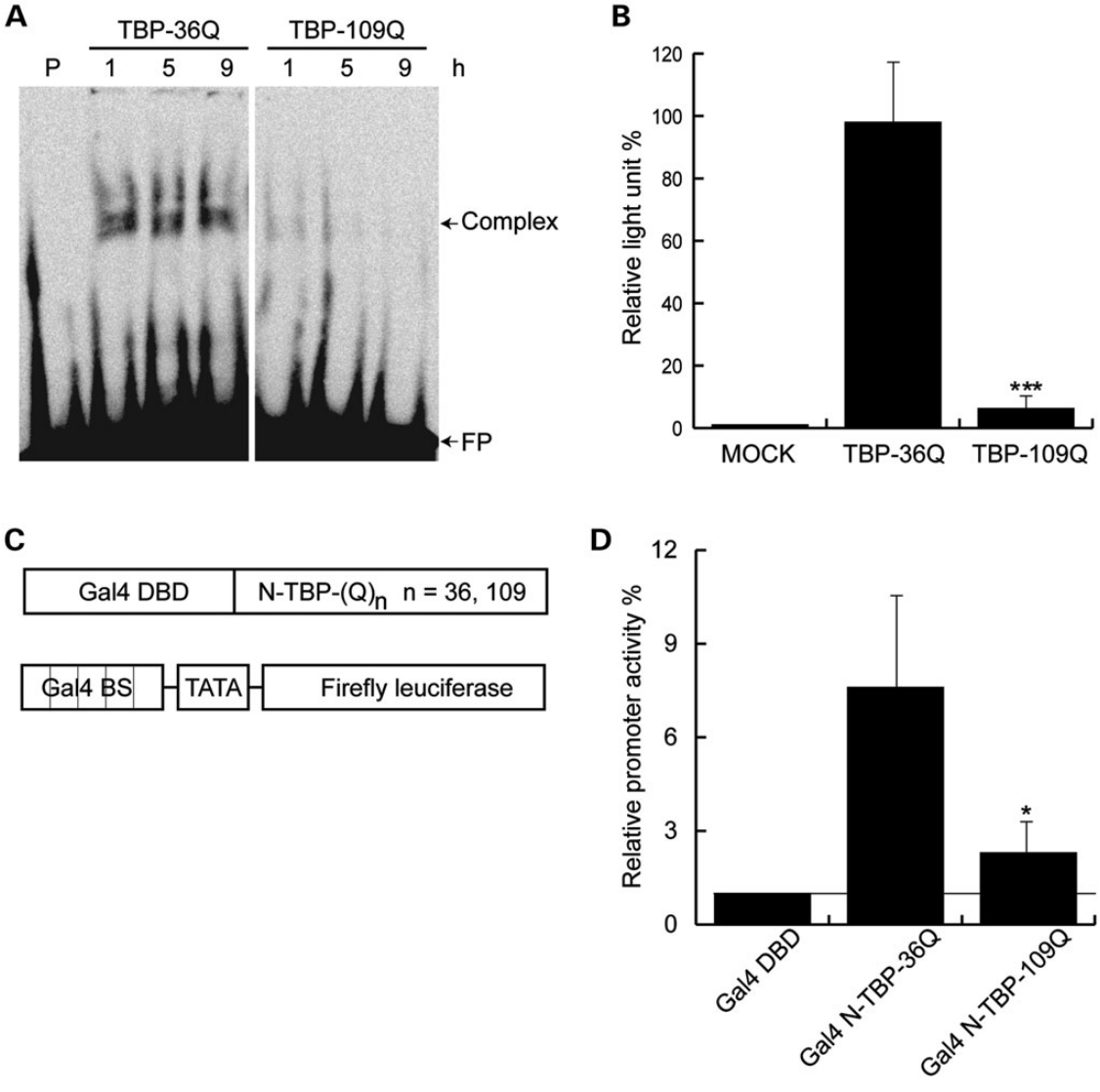

Figure 3. Expanded polyQ affects the function of TBP. (**A**) The effect of the polyQ tract on the DNA-binding ability of TBP was analyzed using EMSA. GST-TBP fusion proteins (1.5 μM) were incubated with a TA-30-B6 DNA linker, and TEV protease was added to initiate the binding reaction for up to 9 h. TBP-36Q bound to the TATA box normally, but TBP-109Q bound significantly less DNA. The binding of TBP-109Q and DNA was completely abolished after 9 h. Control EMSA reactions contained no TBP protein (lane P). Complex, protein–DNA complex; FP, free probe. (**B**) A liquid chemiluminescent DNA pull-down assay showed that TBP-109Q bound significantly less DNA than did TBP-36Q. No protein was added in the MOCK treatment. The relative light unit was calculated by normalizing luciferase to the MOCK treatment. Whether the differences between the two groups were significant was determined the Student's *t*-test (***$P < 0.0001$). (**C**) Schematic depicting the NTD of TBP containing 36Q or 109Q (Gal4 N-TBP-36Q or Gal4 N-TBP-109Q) fused to the Gal4 DBD (upper panel). The reporter construct contained five Gal4 BS and a TATA box fused with firefly luciferase (lower panel). (**D**) TBP-36Q NTD can act as a strong transcriptional activator. TBP-109Q NTD exhibited significantly less transactivation capability. Relative promoter activity was compared by setting the Gal4 DBD to 1. All assays were repeated three times with duplicated samples, and data were expressed as mean ± SD. Statistical significance was determined using the Student's *t*-test (*$P < 0.05$).

detected using a streptavidin–horseradish peroxidase (HRP) conjugate and quantified using chemiluminescence after incubation with HRP substrates. We determined that TBP-36Q bound 15 times more DNA than the same amount of TBP-109Q did (Fig. 3B). This finding is consistent with the aforementioned EMSA results (Fig. 3A and B). The DNA-binding results were also in agreement with those of a previous study in which TBP bearing 71 glutamine residues (TBP-71Q) exhibited considerably less DNA affinity (19). Overall, we concluded that the expanded polyQ tract affected the intrinsic DNA-binding ability of TBP.

TBP contains two functional domains: a saddle-shaped C-terminal domain (CTD) responsible for TATA box DNA binding and a polyQ-rich NTD that exhibits transactivation capability. To test whether polyQ expansion alters the activation capability of TBP NTD, fusion proteins consisting of Gal4 DNA-binding domains (Gal4 DBD) and TBP NTD-36Q (Gal4-N-TBP-36Q) or TBP NTD-109Q (Gal4-N-TBP-109Q) were constructed (Fig. 3C). A firefly luciferase reporter plasmid containing five Gal4 DNA-binding sites (Gal4 BS) upstream of a TATA box was also constructed (Fig. 3C). In transiently transfected HEK293 cells, Gal4-N-TBP-36Q increased the activity of luciferase 7.6-fold, compared with the control Gal4 DBD construct (Fig. 3D). Gal4-N-TBP-109Q also activated the transcription of luciferase; however, its transactivation capability was significantly less than that of Gal4-N-TBP-36Q (Fig. 3D). These results indicated that the transactivation activity of TBP depends on the length of the polyQ tract. Based on the aforementioned findings, we concluded that polyQ expansion impairs both the DNA-binding and transactivation abilities of TBP.

PolyQ-expanded TBP interferes with normal TBP

SCA17 is an inherited autosomal dominant disease. Most sufferers are heterozygotes that carry a normal TBP allele usually bearing 25–38 glutamine residues and a pathogenic TBP allele containing expanded polyQ tracts (43–66Q). Because the interaction of polyQ tracts is length-dependent and normal TBP alleles contain a relatively long polyQ tract, we suspected that pathogenic TBP alleles containing expanded polyQ tracts may interfere with normal TBP. To test this, epitope-tagged TBP was transgenically expressed in the neuroblasts of larval brain lobes driven by *Elav*-gal4. Immunocytochemistry staining showed that the control construct, full-length TBP fused with the C-terminal Flag tag (TBP-36QFL-Flag), was expressed in both the cytoplasm and nuclei of cells (Fig. 4A, upper panel). N-terminal-truncated wild-type TBP containing 36 glutamine residues fused with the Myc tag (N-TBP-36Q-Myc), which was distributed evenly in most neuroblast cells (Fig. 4A, middle panel). Unexpectedly, nuclear inclusions (NIs) were detected in few neuroblasts (~28.6%) that expressed N-TBP-36Q (Fig. 4A, middle panel). The expression of proteins carrying normal polyQ tracts usually does not result in the formation of inclusions in most cell types. We do not know why N-TBP-36Q-Myc formed NIs. We observed that the overexpression of short-repeat-length polyQ proteins formed insoluble aggregates on some occasions (5,29); thus, the formation of polyQ-containing aggregates may be dose-, subcellular localization- or cell type-dependent. Similarly, N-terminal-truncated TBP-109Q (N-TBP-109Q-Myc) formed prominent NIs in the neuroblasts (Fig. 4A, bottom panel). Quantitative analysis revealed that 70.6% of the neuroblasts contained N-TBP-109Q-positive NIs, and 100% of the NIs colocalized with wild-type TBP (Fig. 4A). Because N-TBP-109 formed more NIs with wild-type TBP, the TBP interactions are considered to depend on polyQ length. Notably, the interaction of TBPs was not likely to be caused by dimerization because the carboxy-terminal dimerization domain of TBPs was deleted in both N-TBP-36Q and N-TBP-109Q.

Furthermore, we suspected that the aberrant interaction of TBP may jeopardize its own function. By using liquid chemiluminescent DNA pull-down assays, we determined that truncated TBPs decreased the DNA-binding ability of normal TBP (Fig. 4B). For instance, the addition of N-TBP-36Q decreased the formation of the TBP–DNA complex by 42%, whereas that of N-TBP-54Q decreased the formation of the TBP–DNA complex by 79% (Fig. 4B). This result indicated that polyQ-expanded TBP negatively affected the DNA-binding ability of normal TBP. In transactivation assays, the cotransfection of N-TBP-36Q did not significantly reduce the transactivation capability of normal TBP (Fig. 4C). In contrast, the coexpression of N-TBP-109Q significantly decreased the transcription ability of normal TBP (Fig. 4C). Overall, the findings indicate that polyQ-expanded TBP exhibits a strong propensity to interfere with the function of normal TBP.

Loss of TBP function causes age-associated neurodegeneration in *Drosophila*

As mentioned, polyQ-expanded TBP is dysfunctional, yet it interferes with the function of normal TBP, suggesting that polyQ-expanded TBP may act in a dominant-negative fashion. In other words, apart from the gain-of-toxicity function of mutant TBP, the loss of normal TBP function may also contribute to SCA17 pathogenesis. Thus, loss-of-function mutations in *dTbp* might show SCA17-like neurodegeneration. Several loss-of-function *dTbp* mutant alleles have been recovered from a genetic modifier screen (30). Among all mutant alleles, $dTbp^{sI10}$ is considered to be a protein-null allele because a nonsense mutant was introduced at codon 249, which deletes approximately one-half of the DNA-binding CTD (Supplementary Material, Fig. S1). In addition, the truncated *dTbp* (tr-*dTbp*) protein encoded by the $dTbp^{sI10}$ allele failed to bind TATA box DNA (Supplementary Material, Fig. S2A). The results of a real-time PCR further confirmed that the expression of functional *dTbp* in the heterozygous $dTbp^{sI10}$ mutant was 54.6% of wild-type flies (Supplementary Material, Fig. S2B). Phenotypic analysis revealed that homozygous $dTbp^{sI10}$ mutants die during late embryogenesis (data not shown), but heterozygous $dTbp^{sI10}$ mutants can survive to adulthood without obvious morphological defects. Nevertheless, heterozygous $dTbp^{sI10}$ mutants suffered considerably severe mobility defects (Fig. 5A). Even the newly hatched heterozygous $dTbp^{sI10}$ mutants performed significantly poorer than did wild-type flies of the same age in climbing assays. The mobility defect was sustained throughout the entire lifespan of the flies (Fig. 5A). In addition, the heterozygous $dTbp^{sI10}$ mutants exhibited a shorter lifespan than their wild-type counterparts (Fig. 5B). The average lifespans of the wild-type and heterozygous $dTbp^{sI10}$ flies were 50 and 39 days, respectively.

Although the heterozygous $dTbp^{sI10}$ mutant exhibited no external morphological defects, both reduced mobility and

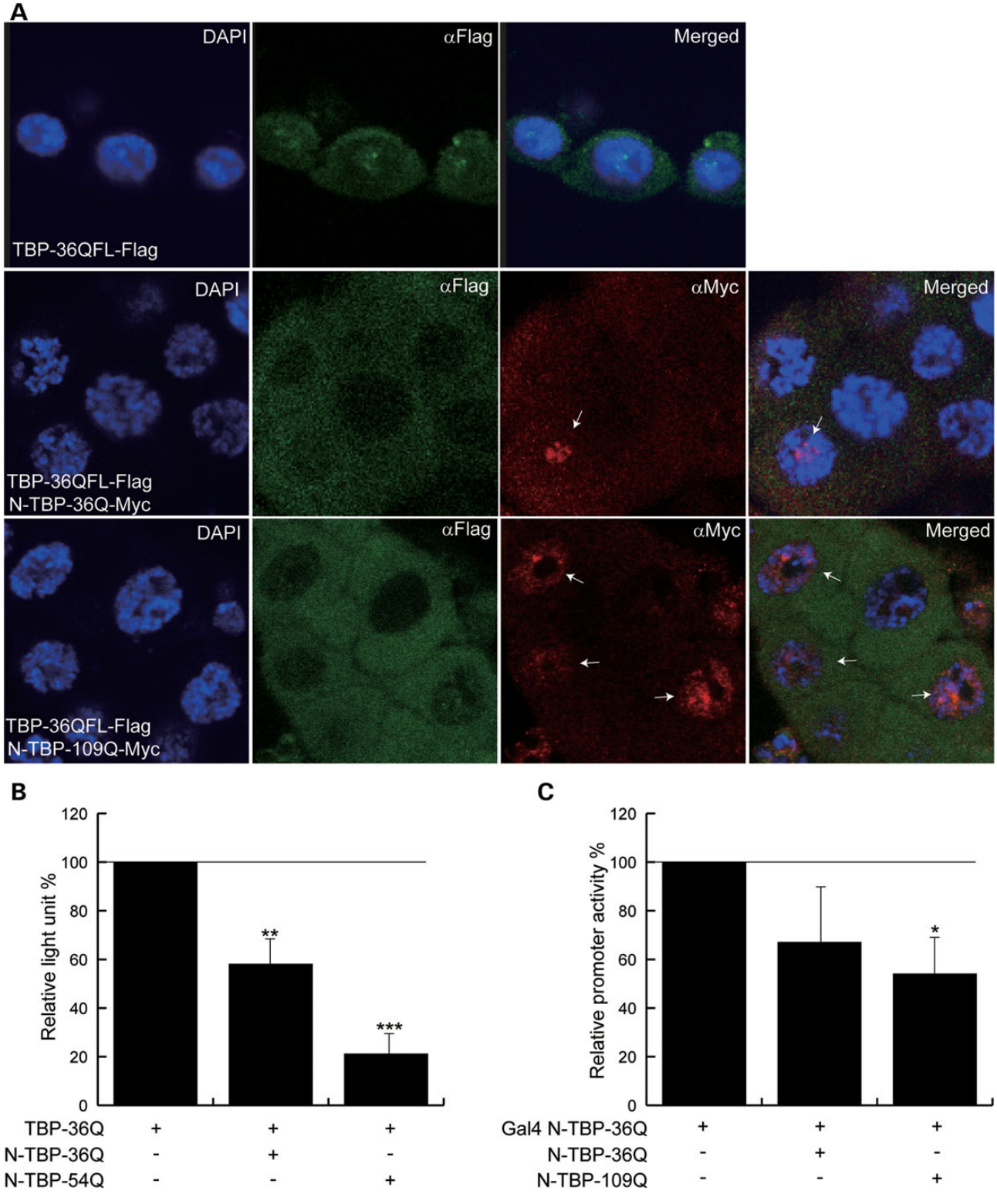

Figure 4. Interaction between polyQ-expanded TBP and normal TBP. (**A**) Control neuroblasts expressing full-length TBP fused with the C-terminal Flag tag (TBP-36QFL-Flag) (upper panel). NTD of TBP-36Q fused with the C-terminal Myc tag (N-TBP-36Q-Myc) colocalized with the TBP-36QFL-Flag in neuroblasts (white arrow, middle panel). Colocalization of TBP-36QFL-Flag and N-TBP-109Q-Myc was detected in the neuroblats (white arrow, bottom panel). (**B**) A liquid chemiluminescent DNA pull-down assay showed that the overexpression of N-TBP-36Q and N-TBP-54Q reduced the transactivation of TBP. All assays were repeated three times with duplicated samples. For comparison, the light unit obtained from TBP-36Q was set at 100% and data were expressed as mean ± SD. Statistical analysis was performed using the Student's *t*-test ($^{**}P < 0.01$; $^{***}P < 0.001$). (**C**). TBP-109Q decreased the transactivation of TBP-36Q. For comparison, the light unit obtained from Gal4 N-TBP-36Q was set at 100% and data were expressed as mean ± SD. Statistical analysis was performed using the Student's *t*-test ($^{*}P < 0.05$).

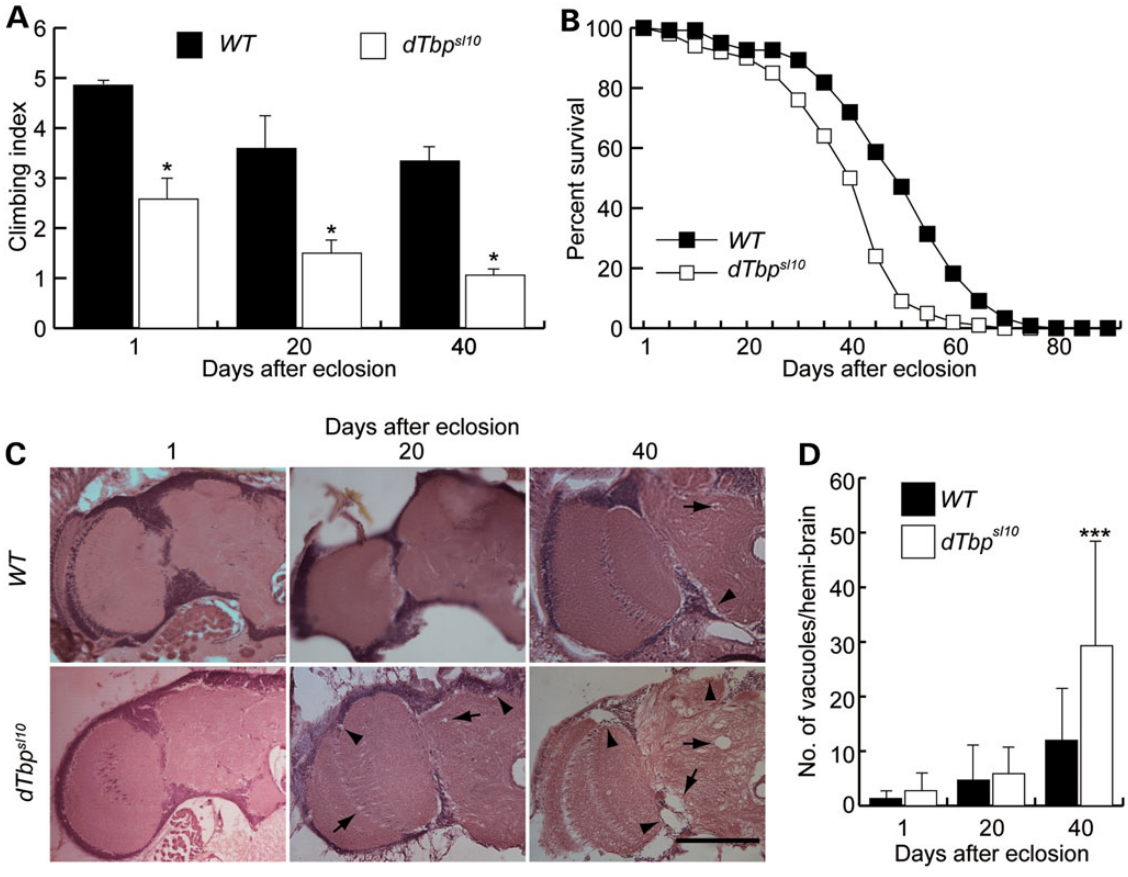

Figure 5. TBP mutant flies. (**A**) Heterozygous *dTbp* mutant flies ($dTbp^{sl10}$) exhibited mobility defects in climbing assays (Student's *t*-test, $^{*}P < 0.05$). (**B**) Heterozygous *dTbp* mutant flies exhibited reduced lifespans (log-rank test, $P < 0.0001$). (**C**) Frontal brain sections of the flies were revealed using H&E staining. Neurodegeneration was detected slightly in the neuropil (arrow) and cortex (arrow head) of control wild-type flies (w^{1118}) that were 40 days old (upper panel). Large and frequent vacuoles were present in the cortex (arrow head) and the neuropil (arrow) of aged *dTbp* mutant flies (lower panel). (**D**) Number of vacuoles in the w^{1118} control (black bar) and heterozygous $dTbp^{sl10}$ (open bar). Neurodegeneration was assessed by quantifying vacuoles in the brains of the flies. Data were expressed as mean ± SD values and were analyzed using the Student's *t*-test ($^{***}P < 0.001$; scale bar = 20 μm).

longevity phenotypes were observed (Fig. 5A and B). Because these age-dependent phenotypes are highly associated with neuronal impairments, we suspected that the downregulation of *dTbp* may disrupt the central nervous system in mutant flies. To test this, hematoxylin and eosin (H&E) staining of adult brain sections was conducted. In the brains of the young wild-type flies, the outer cortex, which consists of basophilic cell bodies of neurons and glia, and the inner neutrophil region, which primarily consists of eosinophilic processes, appeared normal (Fig. 5C). Similarly, no anatomic abnormalities were observed in the nervous systems of the newly eclosed young heterozygous $dTbp^{sl10}$ mutant flies. The gross morphology of the brain, such as the major projection system and brain volume, appeared normal (Fig. 5C). Few and scattered vacuoles were occasionally observed in the brains of the older wild-type flies (Fig. 5C and D). However, compared with wild-type flies of the same age, more and larger vacuoles were observed in the brains of older heterozygous $dTbp^{sl10}$ flies (Fig. 5C and D). Statistical analysis revealed that the number and size of vacuoles significantly increased in the 40-day-old $dTbp^{sl10}$ mutant flies, compared with wild-type flies of the same age (Fig. 5D). Because the formation of brain vacuoles is a characteristic feature of neurodegeneration in *Drosophila*, this result suggested that the downregulation of *dTbp* induced age-dependent neurodegeneration in flies. The neurodegeneration phenotype found in heterozygous $dTbp^{sl10}$ mutant flies is unlikely to be a consequence of the gain-of-toxicity function of tr-*dTbp*, because retinal overexpression of the tr-*dTbp* did not cause degeneration in flies (Supplementary Material, Fig. S3). Because the mobility defect and premature death phenotypes as well as the degeneration phenotype found in $dTbp^{sl10}$ mutants were similar to those found in TBP-109Q-expressing flies, we concluded that a loss of TBP (*dTbp*) function may contribute to SCA17 pathogenesis in flies.

TBP activity modulates the toxicity of polyQ-expanded proteins

To confirm that the deactivation of TBP is a contributing factor of SCA17, the retinal degeneration phenotypes of 7-week-old *Gmr*>TBP-36Q and *Gmr*>TBP-109Q flies in *dTbp* mutant backgrounds were compared. Despite heterozygous *dTbp* mutant flies exhibited reduced lifespan, mobility defect and brain vacuolization (Fig. 5), their external eye morphology appeared normal as seen in the *Gmr*-Gal4 control (Fig. 6, middle panels). It is possible that the neuronal tissues were

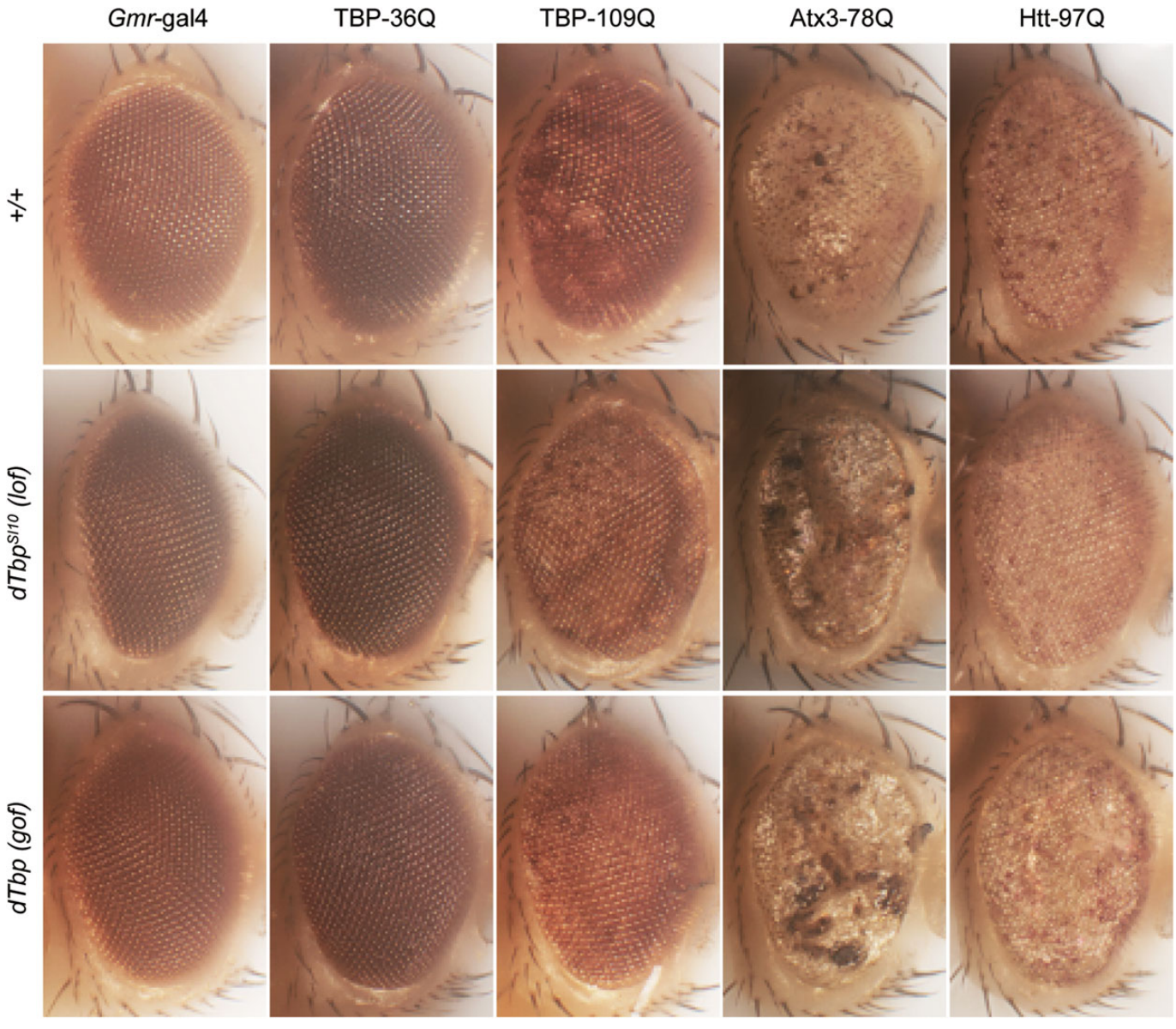

Figure 6. TBP modulates polyQ-induced neurodegeneration. (**A**) The external morphologies of the compound eyes of the 7-week-old males were analyzed. The control *Gmr*-gal4 driver and transgenic flies overexpressing polyQ-containing proteins, including TBP-36Q, TBP-109Q, Atx3-78Q and Htt-97Q, in a wild-type (+/+) background are shown (upper panel). The toxicity of expanded polyQ-containing proteins was enhanced in a heterozygous $dTpb^{sI10}$ mutant (loss-of-function, lof) background (middle panel). The overexpression of *dTbp* (gain-of-function, gof) did not rescue expanded polyQ-induced retinal defects (bottom panel).

more vulnerable to reduced *dTbp*. Similarly, reducing *dTbp* did not enhance the rough-eye phenotype in the *Gmr*>TBP-36Q flies (Fig. 6, upper and middle panels). Overexpressing TBP-109Q caused mild depigmentation in the eyes of flies aged 7 weeks. However, the external ommatidial structures were uneven and large patches of depigmentation appeared in the eyes of the *Gmr*>TBP-109Q flies when *dTbp* was downregulated (Fig. 6, middle panel). This result indicated that loss of TBP function is likely to be involved in SCA17 pathogenesis.

TBP was recruited by mutant Atx3 into NIs in the brains of SCA3 sufferers (5). Moreover, polyQ-expanded Htt inhibited the binding ability of TBP and sequestered TBP into insoluble aggregates, suggesting that deactivated TBP may also be implicated in the pathogenesis of SCA3 and HD (12,31). Similar genetics approaches were performed to address this question. We found that the eyes of the 7-week-old *Gmr*>Atx3-78Q flies exhibited total depigmentation with small, scattered necrotic spots (Fig. 6, upper panel). However, the eyes of the same-aged *Gmr*>Atx3-78Q flies appeared glassy with large necrotic spots in the $dTbp^{sI10}$ mutants (Fig. 6, middle panel). Similarly, the eyes of the 7-week-old *Gmr*>Htt-97Q flies exhibited little depigmentation (Fig. 6, upper panel). The depigmentation phenotype was consistently more severe in the same-aged flies expressing Htt-97Q when *dTbp* was downregulated (Fig. 6, middle panel). Because the toxicities of TBP-109Q, Atx3-78Q and Htt-97Q were all enhanced in $dTbp^{sI10}$ mutant backgrounds, we concluded that the dysfunction of TBP might contribute to SCA17 pathogenesis and the disease progression of SCA3 and HD.

As mentioned, loss of TBP function exacerbated the retinal degeneration induced by various polyQ-expanded proteins, and thus, increasing TBP activity might be beneficial. To address this, we first tested if elevated TBP expression affects eye development in flies because neuronal overexpression of TBP-36Q was found to reduce the lifespan of *Drosophila* (Fig. 1F). Nevertheless, rhabdomere appeared normal and well organized in both the *Gmr*>*dTbp* and *Gmr*>TBP-36Q, *dTbp* flies (Fig. 6, upper and bottom panels). Consistent with this result, eyes of *Gmr*>TBP-36Q were normal till old age (Fig. 1D). These results suggested that eyes might be less sensitive to the elevated TBP than neuronal tissues in *Drosophila*. It is also possible that TBP activity is tightly regulated by forming nonfunctional dimers when it is overexpressed (32). Unexpectedly, the overexpression of *dTbp* did not improve the depigmentation phenotype induced by TBP-109Q expression in the flies (Fig. 6, bottom panel). Moreover, increasing *dTbp* expression enhanced the rough-eye phenotype in Atx3-78Q-expressing flies in which ommatidial collapse and large necrotic spots were consistently observed (Fig. 6, bottom panel). Similarly, the overexpression of *dTbp* induced markedly severe retinal degeneration in the *Gmr*>Htt-97Q flies (Fig. 6, bottom panel). These results suggested that both the down- and upregulation of TBP activity increased the cytotoxicity of the polyQ-expanded proteins.

To analyze the retinal phenotype effectively, the internal ommatidial structure was revealed using confocal microscopy. We determined that the down- or upregulation of *dTbp* did not cause any obvious damage in the internal ommatidial structure of control *Gmr*-gal4 line and flies expressing TBP-36Q (Fig. 7A, first and second columns from the left, and Fig. 7B). The number of rhabdomeres in the retina of the 1-week-old *Gmr*>TBP-109Q flies were reduced slightly (Fig. 7A and B). Unlike the round rhabdomeres of the control flies that were arranged in an asymmetric trapezoid, the rhabdomeres in the retinas of the *Gmr*>TBP-109Q flies appeared oblong and organized in a slightly circular manner (Fig. 7A, arrow, first, second and third columns). Immunocytochemical analysis further revealed that few scattered inclusions which appeared as bright puncta were present in the retinas of the *Gmr*>TBP-109Q flies (Fig. 7A, arrow head). Although the up- or downregulation of *dTbp* did not alter the external morphological phenotype of *Gmr*>TBP-109Q (Fig. 6), decreasing or increasing *dTbp* expression substantially reduced photoreceptors and caused a rhabdomere fusion in the *Gmr*>TBP-109 flies (Fig. 7A, open circle, and Fig. 7B and C). Moreover, additional and large inclusions were observed when *dTbp* was overexpressed (Fig. 7A and C, see arrow head), indicating that TBP activity modulated the disease progression of SCA17.

In the Atx3-78Q-expressing flies, the reiterative hexagonal arrangement of photoreceptor clustering completely disappeared, and numerous protein aggregates appearing as fluorescent foci were observed (Fig. 7). Increasing or decreasing the expression of *dTbp* further reduced the number of photoreceptor cells in the *Gmr*>Atx3-78Q flies (Fig. 7A and B). The average number of photoreceptors in each ommatidium of the *Gmr*>Atx3-78Q and *Gmr*>Atx3-78Q, $dTbp^{sI10}$ and *Gmr* > Atx3-78Q, *dTbp* flies were 1.13, 0.37 and 0.30, respectively (Fig. 7B). Notably, protein aggregate formation seemed to be correlated with TBP activity. Increasing the expression of *dTbp* increased Atx3-78Q aggregate formation, and decreasing the expression of *dTbp* significantly reduced the number of inclusions (Fig. 7A and C). The average number of inclusions in the eyes of the *Gmr*>Atx3-78Q and *Gmr*>Atx3-78Q, $dTbp^{sI10}$ and *Gmr*>Atx3-78Q, *dTbp* flies were 2.54, 1.16 and 7.02 per 400 μm^2, respectively (Fig. 7C). Similar to Atx3-78Q-expressing flies, the internal ommatidial structure of the Htt-97Q-expressing flies was completely disrupted and photoreceptors were substantially reduced (Fig. 7A and B). Up- or down-regulation of *dTbp* expression further lowered the number of photoreceptors in the Htt-97Q-expressing flies (Fig. 7A and B). The average number of photoreceptors in each ommatidium of the *Gmr*>Htt-97Q and *Gmr*>Htt-97Q, $dTbp^{sI10}$ and *Gmr*>-Htt-97Q, *dTbp* flies were 1.27, 0.70 and 0.97, respectively (Fig. 7B). Although the number of Htt-97Q aggregates was non-significantly reduced in the $dTbp^{sI10}$ mutants, such as in the TBP-109Q and Atx3-78Q flies, the overexpression of *dTbp* concomitantly increased aggregate formation in Htt-97Q flies (Fig. 7A and C). These results suggested that TBP activity was highly associated with protein aggregate formation, and that increasing TBP expression may not be beneficial for polyQ-mediated neurodegeneration. Consistent with the findings of this study, short polyQ-containing peptides have been shown to increase the nucleation kinetics of expanded polyQ proteins in a concentration-dependent manner (33). Moreover, the overexpression of short polyQ peptides enhances both aggregate formation and neurotoxicity in *Drosophila* models of HD (33). Overall, we concluded that TBP activity modified the toxicity of polyQ-expanded proteins, and that therapeutic intervention involving the increase of TBP expression may be inadvisable in the treatment of SCA17, SCA3 and HD.

DISCUSSION

Pathogenic studies have indicated that polyQ-expanded TBP forms aggregates, causing transcriptional dysregulation that ultimately leads to SCA17 (19–25). Because the aforementioned pathomechanisms are well documented, we focused on the effect that polyQ expansion has on the function of TBP and its association with SCA17 and other polyQ-mediated diseases. We determined that polyQ expansion within the NTD of TBP affects the DNA-binding ability of its CTD. In addition, we found that TBP-109Q binds significantly less TATA box DNA in both EMSA and liquid chemiluminescent DNA pull-down assays (Fig. 3A and B). The data of this study were consistent with previous findings that have indicated that TBP bearing 71 glutamine residues (TBP-71Q) exhibit little DNA affinity (19). In addition, we determined that polyQ-expanded TBP loses DNA affinity faster than protein aggregates can form (Figs 2B and 3A), suggesting that soluble polyQ-expanded TBP is dysfunctional. The findings seem to agree with the observation that polyQ-expanded Htt in its soluble state rapidly deactivates TBP (31). The results also strengthen the notion that soluble polyQ-expanded proteins are neurotoxic.

We indicated that TBP-109Q exhibited little transcription activity (Fig. 3D). The results seemed to be inconsistent with those of a previous study that showed that TBP with polyQ expansion increased CREB-dependent transcription (18). However, we observed that TBP exhibited the highest CREB activation

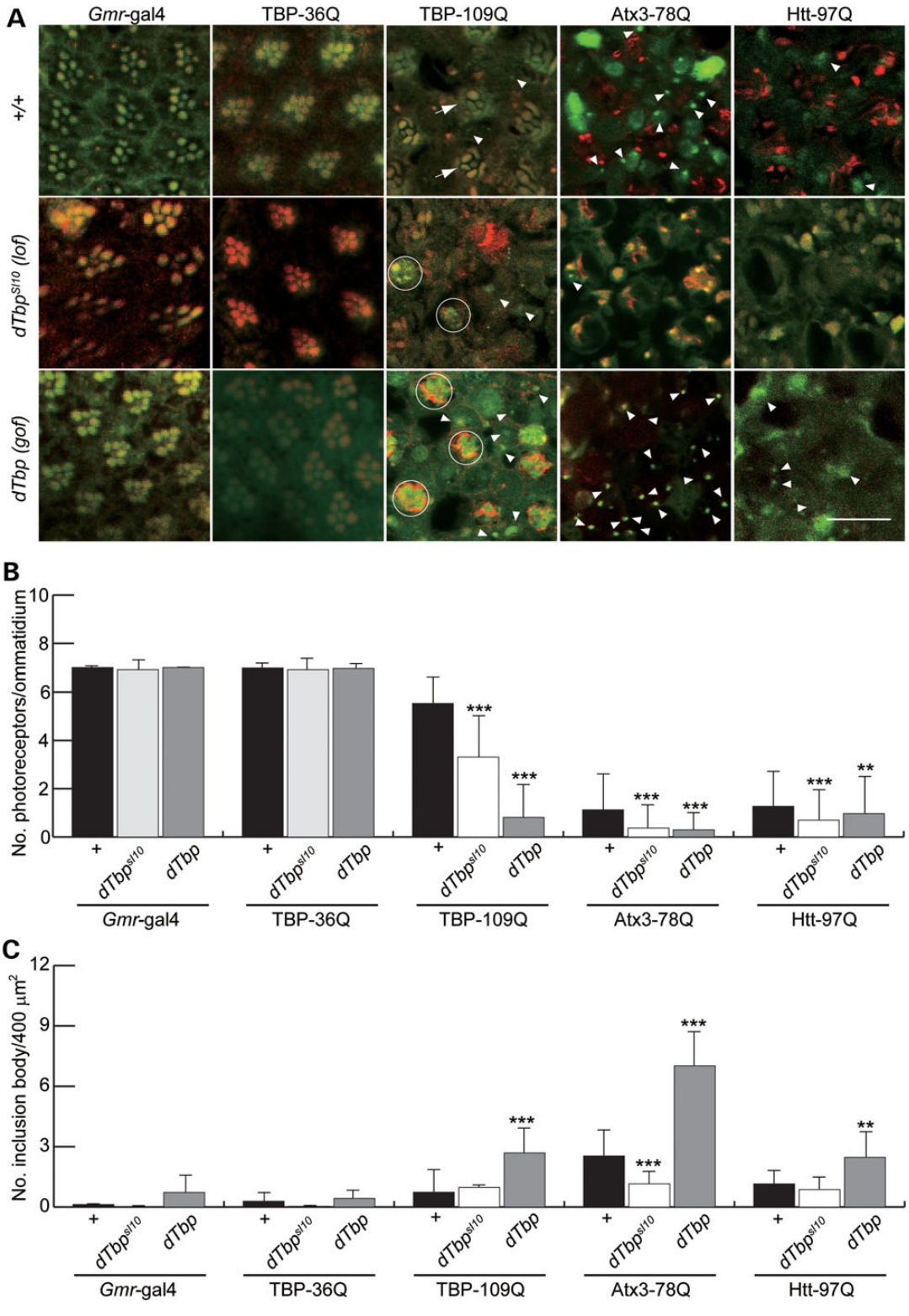

Figure 7. TBP activity correlates with the formation of inclusion. (**A**) Confocal images of tangential sections of retinas from the flies of corresponding genotypes at 7 weeks of age stained with phalloidin (red) and anti-HA (green). The control *Gmr*-gal4 driver and transgenic flies overexpressing polyQ-containing proteins, including TBP-36Q, TBP-109Q, MJD-78Q and Htt-97Q, in a wild-type (+/+) background (upper panel). The toxicity of expanded polyQ-containing proteins was enhanced in a heterozygous $dTpb^{sl10}$ mutant (loss-of-function, lof) background (middle panel). The overexpression of *dTbp* (gain-of-function, gof) did not rescue expanded polyQ-induced retinal defects (bottom panel). Inclusions appeared as green puncta (white arrow heads) and the autofluorescence of eye pigment in rhabdomeres appeared as diffuse green fluorescence. (**B**) The number of photoreceptors (per ommatidium, $n > 170$) and (**C**) inclusion (in an area of 400 μm^2, $n = 5$) in flies expressing expanded polyQ proteins were scored from z-stacked images by using Adobe Photoshop. The data were expressed as mean $\pm$ SD values and were analyzed using the Student's *t*-test ($^*P < 0.05$; $^{**}P < 0.001$ and $^{***}P < 0.001$; scale bar = 10 μm).

when polyQ expansion was moderated (i.e. 48Q). Further increasing the length of the polyQ tracts decreased the transactivation ability of TBP, and the TBP bearing 90 glutamine residues (TBP-90Q) did not stimulate CREB activation (18). Because the polyQ-expanded TBP used in this study contained 109 glutamine residues, the discrepancy in TBP-mediated transcription abilities was attributed to the different lengths of the polyQ within the TBP. In addition to the polyQ-expanded TBP losing its DNA affinity (Fig. 3A and B), we concluded that the function of TBP was polyQ-dependent and that polyQ-expanded TBP was dysfunctional.

Sequence comparisons revealed that TBP exhibited a longer polyQ tract than all the other glutamine-rich proteins in humans (2). Allele frequency studies have shown that, in healthy individuals, TBP usually bears 25–42 glutamine residues, and that >70% of the population carries TBP with 35–38 glutamine residues (18,34,35). Because the oligomerization of polyQ tracts is length-dependent, TBP, which bears a relatively long polyQ tract, is a vulnerable target to attack by pathogenic TBP. The immunochemistry staining performed in this study showed that the pathogenic polyQ-expanded TBP tract exhibited a higher tendency to form NIs than did normal TBP in the brains of *Drosophila* (Fig. 4A). Moreover, polyQ-expanded TBP substantially reduced both the DNA-binding and transactivation abilities of the normal TBP (Fig. 4B and C). These results indicated that the pathogenic TBP interfered with the function of the normal TBP. The results seemed to agree with those of a previous study that found that the pathogenic TBP formed heterodimers with the normal TBP (24). Because intermolecular dimerization requires both molecules to be in proximity, pathogenic TBP must be in close contact and interfere with normal TBP. In addition to the polyQ-expanded TBP being dysfunctional, we argued that the pathogenic TBP may act in a dominant-negative manner, and that the loss of TBP function is a likely causative factor in SCA17.

Though clinical presentations of polyQ-mediated neurodegeneration are heterogeneous, they do show certain commonalities. For instance, certain symptoms of HD overlap with those of DRPLA and SCAs (36). Moreover, SCA17 is alternatively named Huntington's disease-like 4 (HDL4), because polyQ expansion in TBP can phenocopy HD (37,38). These overlapping symptoms can be ascribed to the fact that, in these diseases, the same neuronal tissues are impaired. However, common pathomechanisms are also conceivably operating among these disorders. As mentioned, polyQ-expanded TBP can interact with and deactivate normal TBP (Fig. 4A–C). Accordingly, other polyQ-expanded proteins may also deactivate TBP, causing corresponding neurodegeneration. Because the downregulation of TBP activity worsens rough-eye phenotypes induced by the overexpression of polyQ-expanded proteins (including TBP, Atx3 and Htt), the deactivation of TBP is suggested to be a common causative factor among SCA17, SCA3 and HD (Fig. 6A). Although we did not test whether all the polyQ-expanded proteins disrupted TBP function, observations that polyQ-expanded Htt interacted with and reduced the DNA affinity of TBP (31) and that TBP was sequestered into NIs of polyQ-expanded Atx1, Atx2, Atx3, Atrophin-1 and Htt *in vivo* (5,12) suggested that the inactivation of TBP was a common pathogenic factor in polyQ-mediated neurodegeneration.

The link between dysfunctional TBP and neuronal impairment is currently poorly understood. A previous study reported that the genetic inactivation of the TBP gene caused growth arrest and apoptosis in mice (10). In this study, we showed that abundant and large vacuoles are present in the brains of aged heterozygous *dTbp* mutant flies (Fig. 5C and D). Although we did not provide a direct link between the formation of vacuoles and apoptosis in the brains of aged mutant flies, we did determine that the inactivation of *dTbp* increased the number of apoptotic cells in *Drosophila* during late embryogenesis (Supplementary Material, Fig. S4), indicating that inactivated TBP-induced apoptosis is likely to be conserved in flies and mammals. If the inactivation of TBP is involved in polyQ-mediated disorders, increasing TBP activity might be beneficial. Remarkably, *dTbp* overexpression did not reverse the expanded polyQ-induced rough-eye phenotype, yet it caused severe retinal degeneration in the flies (Figs. 6 and 7A). In addition, the number of insoluble inclusions increased when the *dTbp* was co-overexpressed with mutant-polyQ-containing proteins in the flies (Fig. 7A and C). Consistent with the findings of this study, the overexpression of short polyQ peptides has been shown to enhance both aggregate formation and neurotoxicity in *Drosophila* models of HD by increasing the nucleation kinetics of expanded polyQ proteins in both a concentration- and length-dependent manner (33). This may also explain why overexpression of N-TBP-36Q-Myc formed NIs in the neuroblasts of flies (Fig. 4A, middle panel). These observations strongly suggested that therapeutic intervention by increasing the expression of normal polyQ-containing proteins is inadvisable in the treatment of polyQ-mediated neurodegeneration. In summary, we determined that polyQ expansion altered the function of TBP. Malfunctioning TBP contributed to SCA17 pathogenesis and likely participated in other polyQ-mediated neurodegeneration.

MATERIALS AND METHODS

Fly stocks

Gmr-gal4, *Elav*-gal4 and UAS-Atx3-78Q flies were obtained from the Bloomington Stock Center. The *Drosophila* TBP mutant allele, $dTbp^{s110}$, was a gift from S. Artavanis-Tsakonas (30). Transgenic *Drosophila* expressing UAS-Htt-97Q was obtained from L. Marsh (University of California, Irvine, CA, USA). All of the fly stocks and genetics crosses were maintained and performed at 25°C on standard cornmeal yeast agar media.

DNA constructs and germ-line transformations

TBP-36Q and TBP-109Q were cloned as previously described (23). A 27 amino acid downstream hemagglutinin (HA) tag was fused in-frame to all TBP constructs and subcloned into a pUAST vector as a *Eco*RI–*Not*I fragment (27). To generate a UAS-*dTbp* construct, *Drosophila dTbp* cDNA clone LD44083 (obtained from the *Drosophila* Genome Resource Center) was PCR-amplified using a pair of primers, 5′-CACCATGGACC AAATGCTAAGCC-3′ and 5′-TGACTGCTTCTTGAACTT CTT-3′. The UAS-TBP-36QFL-Flag construct was generated using PCR involving TBP-36Q DNA as the template with a pair of primers, 5′-CACCATGGATCAGAACAACAGCCTG-3′ and 5′-CGTCGTCTTCCTGAATCCCTT-3′. Two N-terminal-truncated TBP constructs, UAS-N-TBP-36Q-Myc and UAS-

N-TBP-109Q-Myc, were generated using PCR involving 5′-CACCATGGATCAGAACAACAGCCTG-3′ and 5′-TGGCGTGGCAGGAGTGATGG-3′ primers. All the amplified DNA fragments were gel-purified and cloned into a pENTR/TEV/D vector to generate Gateway entry clones (Invitrogen). These entry clones were then subcloned into pTWH, pTWF and pTWM vectors for C-terminal HA, Flag and Myc tagging, respectively (http://www.Ciwemb.edu/labs/Murphy/Gatewayvectors.html). All the transgenic DNA constructs were confirmed using sequencing before performing germ-line transformation. A standard germ-line transformation procedure involving w^{1118} as the parental line was followed to generate transgenic flies.

Expression constructs and protein purification

N-terminal-truncated TBPs containing various polyQ repeats, including the DNA of N-TBP-36Q, N-TBP-54Q and N-TBP-109Q, were amplified using PCR involving primers, 5′-CACCATGGATCAGAACAACAGCCTG-3′ and 5′-TTACGTCGTCTTCCTGAATCCCTT-3′. The PCR-amplified DNA was cloned into a pENTR/TEV/D vector by using TOPO cloning technology (Invitrogen) and then into pDEST15 or pDEST17 vectors, causing fusion of an upstream GST or His tag. All the DNA constructs were sequence-confirmed and expressed in *E. coli* BL21 (DE3). To purify the recombinant proteins, bacteria were incubated in an autoinducible medium at 25°C overnight (39). The bacteria were lysed and soluble proteins were purified using affinity chromatography. To express N-terminal-truncated TBP in HEK293T cells, the pSEMS1 vector, which contains an upstream CMV promoter and a Gateway cloning cassette, was used as a destination vector (Covalys Biosciences).

Filter trap assay

Purified GST-TBP proteins were quantified using a protein assay kit (Bio-Rad). Equal amounts of GST-TBP-36Q and GST-TBP-109Q (final concentration = 1.5 μM/each protein) were incubated with 2.5 U of TEV protease (Invitrogen) in a reaction buffer (50 mM Tris, pH 8.0, 0.5 mM EDTA) at 30°C to initiate the proteolytic cleavage of the fusion proteins. The digestion of fusion proteins was completed in 1 h. The reactions were stopped by adding an equal volume of stop solution [4% SDS and 100 mM dithiothreitol (DDT)] at various time points and heating at 95°C for 5 min. The reaction mixture was filtered through a nitrocellulose–acetate membrane (OE66, Schleicher & Schuell). Mouse monoclonal 1C2 antibodies (Chemicon) were diluted in a ratio of 1 : 100 to detect the formation of insoluble aggregates. HRP-conjugated secondary antibodies (Jackson ImmunoResearch) were applied at a dilution of 1 : 10 000. Signals were detected using enhanced chemiluminescence (ECL) kits (Millipore) and captured using an imaging system (GE LAS-3000).

RNA extraction and real-time PCR

Total RNA was extracted from the heads of 1-day-old male flies using the RNeasy Kit (Qiagen) and was then used for reverse transcription using the cDNA reverse transcription kit (Applied Biosystems). A total of 12.5 ng of cDNA were used in Taqman gene expression assays on an StepOnePlus Real-time PCR system (Applied Biosystems). The following probes were used: TBP (assay ID Hs000427620_m1) and Actin (assay ID Dm02371594_s1). Each set of experiments was performed in duplicated and was repeated three times. The comparative C_T method was used for quantification of gene expression.

Immunoblotting

Proteins were extracted from the heads of 30 adult flies in T-PER solution (Pierce). Protein concentrations were quantified using a protein assay kit (Bio-Rad). For each sample, 20 μg of protein was mixed with an equal volume of a 2× Laemmli buffer and denatured at 95°C for 5 min before being resolved in 12% polyacrylamide gels and blotted onto PVDF membranes (Millipore) by using a semidry blotter (Invitrogen). Protein blots were blocked in Tris-buffered saline with 0.1% Tween 20 (Sigma) and 5% dry milk. The primary antibodies used in the study were anti-β-actin (1 : 5000 dilution, GeneTex), anti-TBP antibodies (1 : 200 dilution, Roche), 1TBP18 (1 : 20 000 dilution, QED Bioscience) and 1C2 (1 : 500 dilution, Millipore). HRP-conjugated secondary antibodies (Jackson ImmunoResearch) were diluted in a ratio of 1 : 10 000. ECL substrates were used (Millipore) and images were captured using an imaging system (GE LAS-3000) according to the manufacturer's instructions.

DNA binding

For EMSAs, biotinylated TA-30-B6 DNA comprising a TATA box and 4-nt loop was generated by annealing the synthesized primers 5′-CGGTGTATAAAGCCGCGGTCC-3′ and 5′-GGACCGCCCCTTTATTGACCG-3′ (40). To perform the EMSAs, TA-30-B6 DNA (final concentration = 80 fmole) was mixed with a GST-TBP fusion protein (1.5 μM) in an EMSA buffer (20 mM HEPES–KOH pH 8.0, 150 mM KCl, 4 mM $MgCl_2$, 1 mM DTT, 50 ng/mL of polydI-dC and 5% glycerol). The binding reaction was initiated by adding 2.5 U of TEV protease (Invitrogen) and incubated at 30°C. An aliquot of reaction mixture was withdrawn at each time point and frozen in liquid nitrogen until resolved on a 5% acaryamide gel buffered in 0.5× TBE (45 mM Tris, 45 mM boric acid, 1 mM EDTA and pH 8.0). Biotin-labeled oligomer was electroblotted onto a nylon membrane (Amersham Pharmacia) and detected using a chemiluminescent nucleic acid detection module kit (Pierce). The procedure recommended by the manufacturer was followed and the signal was recorded by scanning using an imager (GE, LAS-3000).

In addition, liquid chemiluminescent DNA pull-down assays were adapted to determine the DNA-binding ability of TBP (28). Purified His-TBP-36Q or His-TBP-109Q was bound to Ni-NTA magnetic beads (Taiwan Advanced Nanotech, Inc.) in binding reactions containing biotinylated TA-30-B6 DNA (1.25 pM) and EMSA buffer (20 mM HEPES–KOH, pH 8.0, 150 mM KCl, 4 mM $MgCl_2$, 1 mM DTT and 5% glycerol) at a final concentration of 0.72 μM at 25°C for 1 h. The bound DNA was captured using a magnet and washed three times with an EMSA buffer without glycerol. Streptavidin-conjugated HRP (Thermo Scientific) was added to the bound DNA in PBT (1 × PBS, 0.1% Triton X-100 and 3% BSA) at 25°C for 1 h. After washing with 1 × PBS three times, the bound DNA was detected using an HRP

substrate. Luminescence was detected using a luminescence microplate reader (BD, SpectraMax L). For binding inhibition, N-terminal-truncated TBP containing 54 glutamine residues (N-TBP-54Q) was used as the truncated TBP-109Q (N-TBP-109) and was highly insoluble. Equal amounts of N-TBP-36Q and N-TBP-54Q were added to the EMSA reactions at a final concentration of 0.72 μM at 25°C for 1 h. The same procedure was then followed to quantify bound DNA.

Cell culture and transactivation assay

The HEK293T cell line was maintained in Dulbecco's modified Eagle's medium supplemented with 10% fetal calf serum at 37°C. The reporter plasmid (pG5Tluc, Fig. 3C) was a generous gift from Dr Y.-S. Huang (Institute of Biomedical Sciences, Academia Sinica) (41). For transfection, equal amounts of reporter plasmid and Gal4 DBD (mock control), Gal4 N-TBP-36Q or Gal4 N-TBP-109Q (1 μg each) were cotransfected into HEK293T cells by using the lipofection method (Lipofectamine 2000, Invitrogen). In inhibitory reactions, equal amounts of reporter plasmid and Gal4 N-TBP-36Q were cotransfected with either 1 μg of N-TBP-36Q or N-TBP-109Q. The transfected cells were incubated for 48 h, and cell lysates were prepared. A dual-luciferase reporter assay system was applied to measure luciferase activity according to the vendor's instructions (Promega). Transactivation activity was expressed as the ratio of firefly luciferase to *Renilla* luciferase. All the transfection experiments were repeated three times with duplicated samples. The difference in luciferase activity was tested using the Student's *t*-test.

Eye morphology

The eye morphology of adult flies was captured using a Leica DMR upright microscope equipped with a digital camera (CoolSNAP 5.0, Photometrics). To increase the depth of field, imaging software was used to create montage composite images (Helicon Focus, HeliconSoft). For SEM, adult fly heads were cut and fixed in 2% glutaraldehyde at 4°C overnight. The samples were briefly rinsed in 1 × PBS (137 mM NaCl, 2.7 mM KCl, 10 mM Na_2HPO_4, 2 mM KH_2PO_4 and pH 7.2) and immersed in 2% osmium acid at room temperature for 5 h. Dehydration was performed using an ethanol series (50, 70, 95 and 100% of ethanol for 30 min each). The fly heads were transferred in 100% acetone at 4°C overnight before critical point drying with liquid CO_2 and being sputter-coated with gold. The images were captured using a JEOL 6400 scanning electron microscope (20 kV, 200 ×).

Histology

The H&E staining of adult fly brain sections was performed as previously described (42). Briefly, *Drosophila* heads were fixed in 4% formalin and dehydrated using an ethanol series. Frontal sections of paraffin-embedded heads were captured using a microtome (Leica RM2135). A series of sections (5 μm) were collected and subjected to H&E staining. The stained samples were visualized and recorded using a microscope (Leica DMR A2) equipped with a digital camera (Photometrics, CoolSnap5.0).

Immunochemistry staining

Dissected eye discs and brain lobes from crawling third-instar larvae were fixed in 4% formaldehyde for 5–10 min. The samples were incubated with the antibodies overnight at 4°C in PBT (1× PBS, 0.1% Triton X-100 and 3% BSA). The primary antibodies used were 1C2 (1 : 100, Chemicon), anti-Flag (1 : 100, Sigma) and anti-Myc (1 : 100, Santa Cruz). FITC- and Cy5-conjugated secondary antibodies (Jackson Immunological Laboratory) were used at a dilution of 1 : 200. Whole-mount immunostainings of adult eyes were performed as described previously (43). Anti-HA antibodies (1 : 200, Sigma) were used to detected inclusions. Rhodamine-conjugated phalloidin (Invitrogen) was used to label F-Actin-enriched rhabdomere according to the manufacturer's instructions. Images were captured and analyzed using a Leica SP2 confocal microscope.

Mobility assay

To test the locomotive functioning of the flies, a graded-climbing assay was applied as described (42,44). For each trial, 10 male flies were tapped down to the bottom of the climbing apparatus and allowed 10 s to climb into scoring areas. All trial sections were repeated 10 times and a total of 50 flies were assayed for each time point. The CI was calculated as follows: $CI = \Sigma(nm)/10$, where n is the number of flies in a given scoring area and m is the score (1–5) for the given score area.

Lifespan analysis

To determine the lifespan of the flies, a group of 10 adult male flies were cultured using standard media in a vial at 25°C. Viable flies were scored and transferred to a food vial at 5-day intervals. At least 200 flies were analyzed for each genotype.

SUPPLEMENTARY MATERIAL

Supplementary Material is available at *HMG* online.

ACKNOWLEDGEMENTS

We thank Y.-S. Huang, S. Artavanis-Tsakonas, L. Marsh, the Bloomington Stock Center, and the *Drosophila* Genomics Resource for the fly stocks, cDNA and reagents. We also thank the Image Core of National Taiwan Normal University and the Electron Microscope Center of National Taiwan University for confocal and SEM imaging.

Conflict of Interest statement. None declared.

FUNDING

This work was supported by National Taiwan Normal University (NTNU100-D-02 and 103T3040B8) and the National Science Council (NSC 101-2311-B-003-002 and NSC 101-2325-003-001).

REFERENCES

1. Duenas, A.M., Goold, R. and Giunti, P. (2006) Molecular pathogenesis of spinocerebellar ataxias. *Brain*, **129**, 1357–1370.
2. Shao, J. and Diamond, M.I. (2007) Polyglutamine diseases: emerging concepts in pathogenesis and therapy. *Hum. Mol. Genet.*, **16** (Spec. 2), R115–R123.
3. Takahashi, Y., Okamoto, Y., Popiel, H.A., Fujikake, N., Toda, T., Kinjo, M. and Nagai, Y. (2007) Detection of polyglutamine protein oligomers in cells by fluorescence correlation spectroscopy. *J. Biol. Chem.*, **282**, 24039–24048.
4. Jiang, H., Nucifora, F.C. Jr, Ross, C.A. and DeFranco, D.B. (2003) Cell death triggered by polyglutamine-expanded huntingtin in a neuronal cell line is associated with degradation of CREB-binding protein. *Hum. Mol. Genet.*, **12**, 1–12.
5. Perez, M.K., Paulson, H.L., Pendse, S.J., Saionz, S.J., Bonini, N.M. and Pittman, R.N. (1998) Recruitment and the role of nuclear localization in polyglutamine-mediated aggregation. *J. Cell. Biol.*, **143**, 1457–1470.
6. Kazantsev, A., Preisinger, E., Dranovsky, A., Goldgaber, D. and Housman, D. (1999) Insoluble detergent-resistant aggregates form between pathological and nonpathological lengths of polyglutamine in mammalian cells. *Proc. Natl. Acad. Sci. USA*, **96**, 11404–11409.
7. Jiang, H., Poirier, M.A., Liang, Y., Pei, Z., Weiskittel, C.E., Smith, W.W., Defranco, D.B. and Ross, C.A. (2006) Depletion of CBP is directly linked with cellular toxicity caused by mutant huntingtin. *Neurobiol. Dis.*, **23**, 543–551.
8. Dunah, A.W., Jeong, H., Griffin, A., Kim, Y.M., Standaert, D.G., Hersch, S.M., Mouradian, M.M., Young, A.B., Tanese, N. and Krainc, D. (2002) Sp1 and TAFII130 transcriptional activity disrupted in early Huntington's disease. *Science*, **296**, 2238–2243.
9. van Roon-Mom, W.M., Reid, S.J., Faull, R.L. and Snell, R.G. (2005) TATA-binding protein in neurodegenerative disease. *Neuroscience*, **133**, 863–872.
10. Martianov, I., Viville, S. and Davidson, I. (2002) RNA polymerase II transcription in murine cells lacking the TATA binding protein. *Science*, **298**, 1036–1039.
11. Huang, C.C., Faber, P.W., Persichetti, F., Mittal, V., Vonsattel, J.P., MacDonald, M.E. and Gusella, J.F. (1998) Amyloid formation by mutant huntingtin: threshold, progressivity and recruitment of normal polyglutamine proteins. *Somat. Cell Mol. Genet.*, **24**, 217–233.
12. van Roon-Mom, W.M., Reid, S.J., Jones, A.L., MacDonald, M.E., Faull, R.L. and Snell, R.G. (2002) Insoluble TATA-binding protein accumulation in Huntington's disease cortex. *Brain Res. Mol. Brain Res.*, **109**, 1–10.
13. Yamada, M., Tsuji, S. and Takahashi, H. (2000) Pathology of CAG repeat diseases. *Neuropathology*, **20**, 319–325.
14. Nakamura, K., Jeong, S.Y., Uchihara, T., Anno, M., Nagashima, K., Nagashima, T., Ikeda, S., Tsuji, S. and Kanazawa, I. (2001) SCA17, a novel autosomal dominant cerebellar ataxia caused by an expanded polyglutamine in TATA-binding protein. *Hum. Mol. Genet.*, **10**, 1441–1448.
15. Fujigasaki, H., Martin, J.J., De Deyn, P.P., Camuzat, A., Deffond, D., Stevanin, G., Dermaut, B., Van Broeckhoven, C., Durr, A. and Brice, A. (2001) CAG repeat expansion in the TATA box-binding protein gene causes autosomal dominant cerebellar ataxia. *Brain*, **124**, 1939–1947.
16. Zuhlke, C. and Burk, K. (2007) Spinocerebellar ataxia type 17 is caused by mutations in the TATA-box binding protein. *Cerebellum*, **6**, 300–307.
17. Gerber, H.P., Seipel, K., Georgiev, O., Hofferer, M., Hug, M., Rusconi, S. and Schaffner, W. (1994) Transcriptional activation modulated by homopolymeric glutamine and proline stretches. *Science*, **263**, 808–811.
18. Reid, S.J., Rees, M.I., van Roon-Mom, W.M., Jones, A.L., MacDonald, M.E., Sutherland, G., During, M.J., Faull, R.L., Owen, M.J., Dragunow, M. *et al.* (2003) Molecular investigation of TBP allele length: a SCA17 cellular model and population study. *Neurobiol. Dis.*, **13**, 37–45.
19. Friedman, M.J., Wang, C.E., Li, X.J. and Li, S. (2008) Polyglutamine expansion reduces the association of TBP with DNA and induces DNA binding-independent neurotoxicity. *J. Biol. Chem.*, **283**, 8283–8290.
20. Lee, L.C., Chen, C.M., Wang, H.C., Hsieh, H.H., Chiu, I.S., Su, M.T., Hsieh-Li, H.M., Wu, C.H., Lee, G.C., Lee-Chen, G.J. *et al.* (2012) Role of the CCAAT-binding protein NFY in SCA17 pathogenesis. *PLoS ONE*, **7**, e35302.
21. Ren, J., Jegga, A.G., Zhang, M., Deng, J., Liu, J., Gordon, C.B., Aronow, B.J., Lu, L.J., Zhang, B. and Ma, J. (2011) A Drosophila model of the neurodegenerative disease SCA17 reveals a role of RBP-J/Su(H) in modulating the pathological outcome. *Hum. Mol. Genet.*, **20**, 3424–3436.
22. Chen, C.M., Lee, L.C., Soong, B.W., Fung, H.C., Hsu, W.C., Lin, P.Y., Huang, H.J., Chen, F.L., Lin, C.Y., Lee-Chen, G.J. *et al.* (2010) SCA17 repeat expansion: mildly expanded CAG/CAA repeat alleles in neurological disorders and the functional implications. *Clin. Chim. Acta*, **411**, 375–380.
23. Lee, L.C., Chen, C.M., Chen, F.L., Lin, P.Y., Hsiao, Y.C., Wang, P.R., Su, M.T., Hsieh-Li, H.M., Hwang, J.C., Wu, C.H. *et al.* (2009) Altered expression of HSPA5, HSPA8 and PARK7 in spinocerebellar ataxia type 17 identified by 2-dimensional fluorescence difference in gel electrophoresis. *Clin. Chim. Acta*, **400**, 56–62.
24. Friedman, M.J., Shah, A.G., Fang, Z.H., Ward, E.G., Warren, S.T., Li, S. and Li, X.J. (2007) Polyglutamine domain modulates the TBP-TFIIB interaction: implications for its normal function and neurodegeneration. *Nat. Neurosci.*, **10**, 1519–1528.
25. Huang, S., Ling, J.J., Yang, S., Li, X.J. and Li, S. (2011) Neuronal expression of TATA box-binding protein containing expanded polyglutamine in knock-in mice reduces chaperone protein response by impairing the function of nuclear factor-Y transcription factor. *Brain*, **134**, 1943–1958.
26. Yang, S., Huang, S., Gaertig, M.A., Li, X.J. and Li, S. (2014) Age-dependent decrease in chaperone activity impairs MANF expression, leading to Purkinje cell degeneration in inducible SCA17 mice. *Neuron*, **81**, 349–365.
27. Brand, A.H. and Perrimon, N. (1993) Targeted gene expression as a means of altering cell fates and generating dominant phenotypes. *Development*, **118**, 401–415.
28. Iwasaki, T., Miyazaki, W., Rokutanda, N. and Koibuchi, N. (2008) Liquid chemiluminescent DNA pull-down assay to measure nuclear receptor-DNA binding in solution. *Biotechniques*, **45**, 445–448.
29. Invernizzi, G., Aprile, F.A., Natalello, A., Ghisleni, A., Penco, A., Relini, A., Doglia, S.M., Tortora, P. and Regonesi, M.E. (2012) The relationship between aggregation and toxicity of polyglutamine-containing ataxin-3 in the intracellular environment of *Escherichia coli*. *PLoS ONE*, **7**, e51890.
30. Verheyen, E.M., Purcell, K.J., Fortini, M.E. and Artavanis-Tsakonas, S. (1996) Analysis of dominant enhancers and suppressors of activated Notch in Drosophila. *Genetics*, **144**, 1127–1141.
31. Schaffar, G., Breuer, P., Boteva, R., Behrends, C., Tzvetkov, N., Strippel, N., Sakahira, H., Siegers, K., Hayer-Hartl, M. and Hartl, F.U. (2004) Cellular toxicity of polyglutamine expansion proteins: mechanism of transcription factor deactivation. *Mol. Cell*, **15**, 95–105.
32. Jackson-Fisher, A.J., Chitikila, C., Mitra, M. and Pugh, B.F. (1999) A role for TBP dimerization in preventing unregulated gene expression. *Mol. Cell*, **3**, 717–727.
33. Slepko, N., Bhattacharyya, A.M., Jackson, G.R., Steffan, J.S., Marsh, J.L., Thompson, L.M. and Wetzel, R. (2006) Normal-repeat-length polyglutamine peptides accelerate aggregation nucleation and cytotoxicity of expanded polyglutamine proteins. *Proc. Natl. Acad. Sci. USA*, **103**, 14367–14372.
34. Schols, L., Bauer, P., Schmidt, T., Schulte, T. and Riess, O. (2004) Autosomal dominant cerebellar ataxias: clinical features, genetics, and pathogenesis. *Lancet Neurol.*, **3**, 291–304.
35. Chen, C.M., Lane, H.Y., Wu, Y.R., Ro, L.S., Chen, F.L., Hung, W.L., Hou, Y.T., Lin, C.Y., Huang, S.Y., Chen, I.C. *et al.* (2005) Expanded trinucleotide repeats in the TBP/SCA17 gene mapped to chromosome 6q27 are associated with schizophrenia. *Schizophr. Res.*, **78**, 131–136.
36. Wild, E.J., Mudanohwo, E.E., Sweeney, M.G., Schneider, S.A., Beck, J., Bhatia, K.P., Rossor, M.N., Davis, M.B. and Tabrizi, S.J. (2008) Huntington's disease phenocopies are clinically and genetically heterogeneous. *Mov. Disord.*, **23**, 716–720.
37. Stevanin, G., Fujigasaki, H., Lebre, A.S., Camuzat, A., Jeannequin, C., Dode, C., Takahashi, J., San, C., Bellance, R., Brice, A. *et al.* (2003) Huntington's disease-like phenotype due to trinucleotide repeat expansions in the TBP and JPH3 genes. *Brain*, **126**, 1599–1603.
38. Stevanin, G. and Brice, A. (2008) Spinocerebellar ataxia 17 (SCA17) and Huntington's disease-like 4 (HDL4). *Cerebellum*, **7**, 170–178.
39. Studier, F.W. (2005) Protein production by auto-induction in high density shaking cultures. *Protein Expr. Purif.*, **41**, 207–234.
40. Grove, A., Galeone, A., Yu, E., Mayol, L. and Geiduschek, E.P. (1998) Affinity, stability and polarity of binding of the TATA binding protein governed by flexure at the TATA Box. *J. Mol. Biol.*, **282**, 731–739.

41. Chang, C. and Gralla, J.D. (1993) Properties of initiator-associated transcription mediated by GAL4-VP16. *Mol. Cell. Biol.*, **13**, 7469–7475.
42. Wang, Y.C., Lee, C.M., Lee, L.C., Tung, L.C., Hsieh-Li, H.M., Lee-Chen, G.J. and Su, M.T. (2011) Mitochondrial dysfunction and oxidative stress contribute to the pathogenesis of spinocerebellar ataxia type 12 (SCA12). *J. Biol. Chem.*, **286**, 21742–21754.
43. Chang, Y.C., Hung, W.T., Chang, H.C., Wu, C.L., Chiang, A.S., Jackson, G.R. and Sang, T.K. (2011) Pathogenic VCP/TER94 alleles are dominant actives and contribute to neurodegeneration by altering cellular ATP level in a *Drosophila* IBMPFD model. *PLoS Genet.*, **7**, e1001288.
44. Todd, A.M. and Staveley, B.E. (2004) Novel assay and analysis for measuring climbing ability in *Drosophila*. *Drosophila Infor. Serv.*, **87**, 101–107.